



Combined mild and hard novel fabrication approach for nanoporous membrane

Gurpreet Singh Walia¹ · Harminder Singh¹ · Jasleen Kaur¹ · Manoj Kumar Kushwaha² · Anupinder Singh¹ · N. S. Saini¹

Received: 10 September 2018 / Accepted: 3 September 2019 / Published online: 26 September 2019
© The Brazilian Society of Mechanical Sciences and Engineering 2019

Abstract

Anodization of aluminum by a hard anodizing or mild anodizing process is usually done to obtain metal top surface finishing. Recently, this process has been becoming famous for the formation of through-hole porous oxide membranes (TH-POM) which act as a template for fabrication of nanowires/tubes. Membranes with different pore diameters, interpore distance, depth of pore and porosity can be obtained by selecting different parameters such as type and concentration of electrolyte, pH, temperature, time and applied voltage. In this research paper, exclusive experiments were studied and conducted to obtain TH-POM which will be template for generation of ordered nanowires by an electrochemical process. This research is carried out using a combination of mild anodization (MA) and hard anodization (HA) with novel heterogeneous control parameters by using DC power supply, magnetic stirrer and data acquisition system (DAQ) and at high temperature in order to minimize the refrigeration cost required for cooling the electrolyte. Excellent ordered membranes of 24–29 nm and 40–50 nm pore diameter were obtained in short time, characterized by SEM and EDS and analyzed by I – V curves obtained using an Arduino-based current/voltage data logger. A thermal stress test is also performed on the TH-POM formed using MA and HA.

Keywords Anodization · Oxalic · Porous · Membrane · Sulfuric · Aluminum · Nano · Wires

1 Introduction

Back to the beginning of the last century, anodization was used to protect seaplane parts made up of aluminum alloys (duralumin) against corrosion. Anodic aluminum in the form of alumina (Al_2O_3) is processed by an electrochemical method which has proved to be a very successful process. An oxide layer on aluminum has lower thermal conductivity and five times less coefficient of linear expansion than basic metal [1]. Anodization process also exists for other metals such as Ti [2, 3], Zn [4], Mg [5], Nb, Zr, Hf and Ta [6]. However, a number of applications

have been explored using the anodized aluminum oxide as compared to other anodized metals including dielectric films for capacitor [7], coloring and decoration [8], template-based fabrication of nanotubes using CVD method and sol–gel method [9, 10], filtration and separation of chemicals in laboratory, optimization of pool-boiling performance [11], IDT sensors [12–14], etching template, acting as a template for electrodeposition of various metals in the pores resulting in nanowires [15] and FePt nanodot [16], and fabrication of MEMS devices [17]. TH-POM template is a close-packed array of hexagonal cylindrical cells with a pore in the center of each cell. Controlling the parameters of TH-POM such as pore diameter, interpore distance, depth, time and temperature is very much easy and cheap, hence advantageous in controlling properties of nanostructured materials. Nanostructure shape and geometry of pores are controlled via electrochemical anodization process [18]. Parameters such as applied DC potential and acid (type and concentration) contribute to the formation of the porous nanostructures with various pore diameters D_{pore} , interpore distances $D_{\text{interpore}}$, porosity % and pore densities. The growth rate of TH-POM

Technical Editor: Márcio Bacci da Silva, Ph.D.

✉ Gurpreet Singh Walia
gurpreet509@gmail.com

✉ Harminder Singh
harminder10@gmail.com

¹ Guru Nanak Dev University, Amritsar, Punjab, India

² Shaheed Bhagat Singh State Technical Campus, Ferozepur, Punjab, India

nanostructure depends on the temperature of electrolyte; at higher temperature, the growth rate is fast, whereas at lower temperature the growth rate slows down. Fan et al. discussed that a barrier layer at the pore bottom has a strong shielding effect on the growth of anodic alumina [19]. Stepniowski et al. reported that laser pre-treated technical purity aluminum influences the aluminum substrate but has no influence on the growth rate mechanism of oxide when subjected to anodizing in sulfuric acid [20].

Different methods of anodization are: first-step, pre-imprinting, second-step and multi-step anodization. First-step anodization is usually performed in acids such as H_2SO_4 , $\text{C}_2\text{H}_2\text{O}_4$, H_3PO_4 , H_2CrO_4 , H_3BO_3 and $\text{C}_6\text{H}_8\text{O}_7$, which results in non-uniformity of pore diameter and inter-pore distance. Pre-imprinting anodization is a process of inscribing multiple array pore patterns on the Al surface using techniques such as pressing imprints, UV exposure and e-beam lithography. In recent studies, multi-step anodization has resulted in the formation of uniform self-organized nanopores on Al substrates. Masuda et al. described a two-step replication method carried out for 160 h at 0 °C in oxalic acid [21]. Hui et al. prepared AAO template on silicon substrate using two-step anodization in only oxalic acid at 40 V until aluminum layer sputtered on Si wafer was completely transferred into Al_2O_3 [22]. The second-step anodization can be performed using either homogeneous (same) or heterogeneous electrolytes.

In recent studies, a through-hole porous oxide membrane (TH-POM) has been popularly used for the fabrication of nanowires of various metals and composites such as Cu, Ni, Ni–Cr, Co, Au and Pt because of the self-ordered hexagonal property of pores. The fabrication of TH-POM can be done by using either mild anodization (MA) or hard anodization (HA). The mild anodization utilizes low anodizing currents (< 5–10 mA) and produces self-ordered pores, but it is a slow process and operated for 12 h or more. Recently, Maghsodi et al. have used oxalic acid in addition to sulfuric acid during the process to fabricate AAO template [23]. Masuda et al. employed a two-step mild anodization technique on the surface of aluminum initiated by a texture pattern generated by SiC mold [21, 24]. The hard anodization is a faster process and works on higher voltages/higher currents (> 50 mA), but it produces films with disordered pore structures because of high current flow during anodization through the electrolyte, and temperature of the electrolyte becomes high which leads to non-uniform formation of pores or can crack the material too [25, 26]. Chu et al. [27] reported a single-step hard anodization process using sulfuric acid solution at 40–70 V. Lee et al. [28] worked on pre-existed oxide film and employed HA using oxalic acid at 110–150 V. Liu et al. [29] prepared the AAO by the first step employing HA in H_2SO_4 and second step MA in oxalic acid for more than 4 h.

The motivation of this work is to lower the time taken for the anodization process and reduce the refrigeration cost for cooling the electrolyte by using a combination of HA and MA with novel heterogeneous electrolyte parameters. Figure 1a–j demonstrates the stepwise flow of experiment. In the first step, MA in sulfuric acid for 40 min is employed to obtain the array of concaves. For the second step, HA in oxalic acid is performed for less than 2 h. The transformation of pore formation from MA to HA is discussed. The combination of MA, HA and heterogeneous electrolyte not only has proved to be cost-effective and time-saving process but also increases the strength against thermal stress of TH-POM, which was also tested by heating the membrane over hot plate. In the following sections of this paper, we have provided all information about anodization such as preparation of sample for anodization, removal of remaining aluminum substrate and preparation of samples for characterization, which is not transparently presented by the previous researchers, analyzed the AAO pore formation and studied the pore formation mechanism with the help of current–voltage graphs.

2 Materials and methods

An aluminum sheet, 0.2 mm thick, was cut into 6 cm × 3 cm pieces out of which 2 cm² area was selected by masking rest of the area with the help of non-conducting tape (so that electrolyte affects only the unmasked area) for anodization process as shown in Fig. 1a, b. The samples were washed with detergent and dipped in 4 g NaOH in 100 ml deionized (DI) water solution until the solution becomes white milky color. Ultrasonication of the above cleaned samples was performed in acetone at 65% amplitude for 5 min and in DI at 75% amplitude for 5 min sequentially. Prior to anodization, electropolishing was performed on cleaned samples in standard solution of 1:4 ratio of perchloric acid (HClO_4) and ethanol ($\text{C}_2\text{H}_6\text{O}$) in a two-electrode electrochemical cell operated at 20 V for 4 min at room temperature. After rinsing the electropolished samples in isopropylamine (IPA), acetone and DI water, samples were dried for 12 h.

In the first step, mild anodization (MA) was performed in an electrochemical cell using electrolyte prepared as 2.94 ml sulfuric acid (H_2SO_4) in 147.06 ml DI water. The electrochemical cell was operated at 20 V using self-designed DC power supply (variable 30 V, 2 A) for 40 min at room temperature, in which above prepared samples act as anode and another aluminum plate acts as cathode (counter electrode). The distance between two electrodes was adjusted at 30 mm, and area of counter electrode exposed in electrolyte must be greater than twice the area of working electrode (in this case ≥ 2 cm²). The anodized samples were rinsed with DI water and air-dried for 1 h. It was observed that an oxide

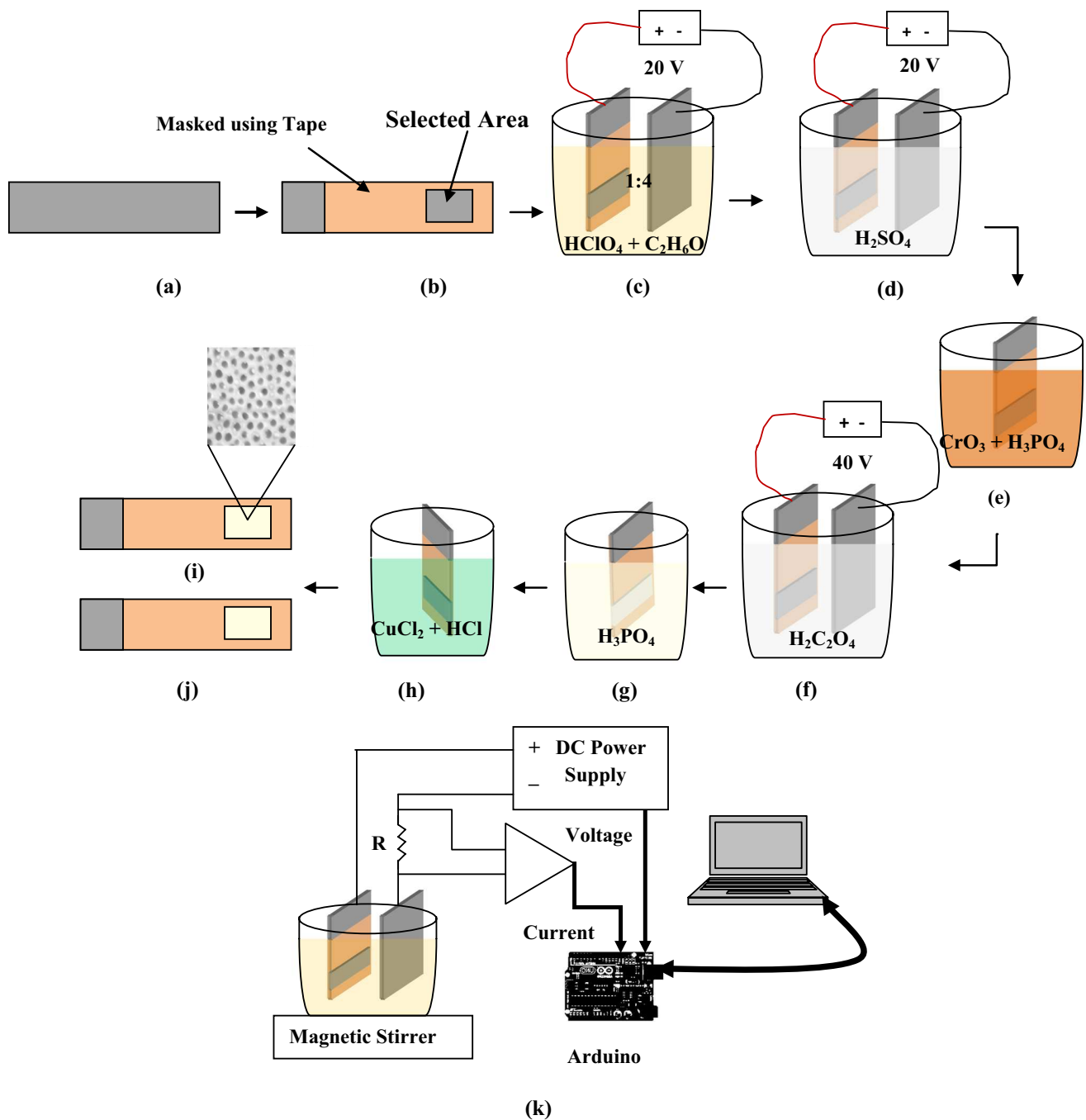


Fig. 1 Schematic diagram showing the flow of experiment and experimental setup. **a** Cleaned aluminum sample; **b** masking the sample for further process; **c** electropolishing of aluminum sample at 20 V; **d** first-step MA performed in 0.3 M sulfuric acid at 20 V; **e** etching of oxide layer after the first step; **f** second-step HA in oxalic acid at

40 V; **g** pore widening in orthophosphoric acid for 10 min; **h** backside aluminum removal in mixture of copper(II) chloride and hydrochloric acid; **i, j** front and backsides of a through-hole porous oxide membrane, respectively; **k** power supply unit with a data logger

layer has been formed on the surface and confirmed scientifically with the help of multi-meter that the surface was non-conductive. The variation in voltage and current density was recorded for further analysis in computer using an Arduino-based data logger as shown in Fig. 1k.

To dissolve the oxide layer, samples were immersed in etchant solution prepared by mixing 2 g of chromic acid in 100 ml of DI and 7 ml of orthophosphoric acid in 93 ml of DI, maintaining the temperature between 64 and 80 °C for 30 min. It was observed that the oxide layer has been removed and

dimples or array of concaves were formed on the top surface of the samples which leads to formations of self-ordered pores.

After rinsing the samples in IPA and DI to remove chromic particles from the surface and then drying the samples, the second-step hard anodization (HA) was performed in 6.61 g oxalic acid in 175 ml DI for 1.5 h using DC power supply at 40 V, maintaining the temperature less than 15 °C. After operating the setup for 1.5 h, voltage was intentionally decremented at 1 V/60 s in order to reduce the barrier layer thickness which is beneath the pores, and then operated the setup for next 20 min at 15 V.

The samples so obtained were non-conductive in nature and immersed in solution prepared by mixing 11.76 ml H₃PO₄ in 88.24 ml DI for 10 min to widen the pores. These samples were then washed properly with IPA, acetone and DI to remove any chemical remaining on the sample.

In order to obtain the through-hole porous oxide membrane (TH-POM) which is free from aluminum substrate, the portion that was treated with electrolyte must be protected using some epoxy or such material which can be dissolved in later stage easily without affecting the membrane. In this experiment, nail polish was used which can be easily removed using acetone later on [30]. However, Masuda et al. reported a protective layer made of a mixture of nitrocellulose and polyester resin in ethyl acetate, butyl acetate and heptanes [31]. The covered side of the sample was placed on the glass slide, and backside of membrane was put in contact with a mixture of 5 g CuCl₂, 50 ml DI and 10 ml HCl solution. After this process, the left over copper on the membrane surface was cleaned by immersing it in HNO₃. After drying the membrane in air as shown in Fig. 6a, the morphological parameters of membrane were studied using scanning electron microscopy (Zeiss Gemini SEM) and EDS available at Guru Nanak Dev University, Amritsar, Punjab, India. The porosity was calculated from the ratio:

$$\text{Porosity}\% = \frac{\pi}{2\sqrt{3}} \left(\frac{D_{\text{Pore}}}{D_{\text{interpore}}} \right)^2 \times 100 \quad (1)$$

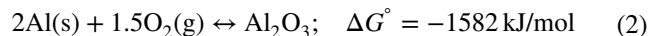
where D_{pore} is the diameter of pores and $D_{\text{interpore}}$ is the distance between two adjacent pores.

The procedure adopted for anodization is presented in Table 1.

Thermal testing of some of the prepared anodized samples was done on a hot plate at various temperatures to test its suitability under thermal stress conditions. This testing was done on samples before removing the aluminum substrate (opposite part of oxide layer, as discussed above). The samples were tested at varying temperatures up to 150 °C.

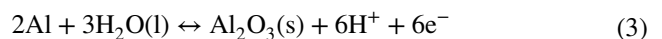
3 Results and discussion

Aluminum is a reactive metal which reacts spontaneously with water/air to form a corrosion-protective aluminum oxide layer whose thickness is of the order of 4 nm. The formation of aluminum oxide in air can be ascribed to large negative Gibb's free energy changes given by the following equation [32]:



In order to form a stable and thick oxide layer for the application in the field of nanostructure fabrication, aluminum is electrochemically anodized in different electrolytes. In this work, the electrolyte is dilute sulfuric acid and oxalic acid (acidified water), which dissociates into hydrogen ions and oxygen ions on the application of potential as described in Eq. (6). The process starts with the O²⁻ ions present in the electrolyte which reacts with the surface of the Al to remove the Al³⁺ ions (Fig. 2j).

The oxide grows at an anode electrode known as oxidation reaction,



The hydrogen ions (H⁺) are attracted toward the negative cathode and are discharged as hydrogen gas:

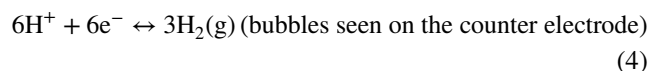


Table 1 Steps of formation of TH-POM

Step 1	Sample cleaning	Washing with detergent and NaOH–DI water ultrasonication in acetone
Step 2	Electropolishing	After cleaning electropolishing in 1:4 ratio of perchloric acid (HClO ₄) and ethanol at 20 V for 4 min at 20 °C. Rinsing the electropolished samples in IPA, acetone and DI water
Step 3	First anodization	Anodization in H ₂ SO ₄ at 20 V for 40 min
Step 4	Oxide dissolution	Immersion in a mixture of chromic acid and orthophosphoric acid at 64–80 °C for 30 min
Step 5	Second anodization	Anodization in oxalic acid at 40 V for 1.5 h and less than 15 °C After 1.5 h, voltage decremented at 1 V/60 s and then operated the setup at 15 V for 20 min
Step 6	Pore widening	Immersion in H ₃ PO ₄ for 10 min and then washing with IPA, acetone, and DI
Step 7	Preparation of TH-POM	Backside of membrane was put in contact with a mixture of CuCl ₂ and HCl solution and then cleaned with HNO ₃

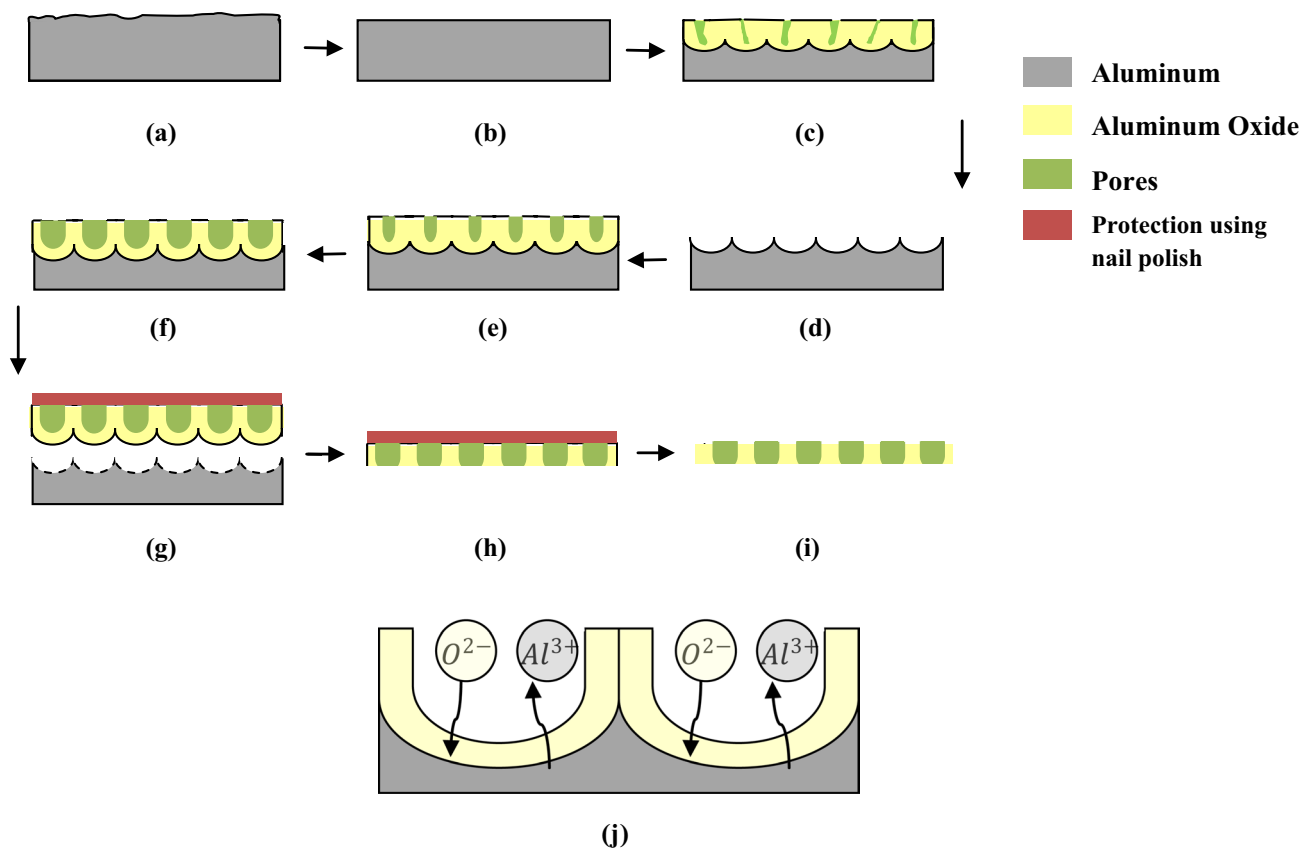


Fig. 2 Schematic diagram of the resultant sample: **a** pure aluminum; **b** electropolished aluminum; **c** non-uniform pores after the first step; **d** removal of non-uniform oxide layer; **e** well-ordered pores after the

second step; **f** pore widening; **g** dissolution of bottom part of alumina layer; **h** removal of barrier layer; **i** porous oxide membrane; **j** formation and dissolution of oxide layer

The samples fabricated in this study were characterized after mild anodization (MA). Figure 2 shows a schematic diagram of the resultant sample at each stage of experiment. Aluminum was anodized at various potentials (20 V and 40 V) in two different electrolytes sequentially, resulting in maximum 49 mA cm^{-2} current density (Fig. 5a) during the process to form highly ordered TH-POM. The SEM micrographs of samples under mild anodization (MA) and hard anodization (HA) in combination with different electrolytes, i.e., sulfuric acid and oxalic acid, are presented in Fig. 3. Before taking FE-SEM images, samples were prepared with the following procedure. A thin layer of gold was sputtered on the non-conductive surface of TH-POM (50 mA current and 40 s, parameters for sputtering) before characterization. Figure 3a shows the top view FE-SEM images of TH-POM prepared in H_2SO_4 at 20 V for 10 to 40 min. It can also be observed from Fig. 3a (i–v) that time has a significant effect on the formation of pores and the size of pores has been increased from 6 to 24 nm (from 10 to 40 min), resulting in an increase in the porosity from 0.5 to 10%. The relationship between the pore diameter and applied potential, i.e., 1.2 nm V^{-1} , is found to be same as per literature [33–35].

The white portion in Fig. 3a (v) shows the deposition of Au particles in some pores. The increase in time duration of anodization is directly proportional to the increase in pore diameter as shown in Fig. 3a (i–v), but precautions must be taken as longer time duration may damage the sample too. It is noticed from Fig. 3a that a less ordered pore texture is fabricated in small duration anodization of samples, and as shown in Fig. 3a (v), pores are more uniform, equally spaced and in hexagonal pattern for longer duration. The first-step anodization was also carried out unintentionally with oxalic acid, which resulted in heat generation on the surface of the electrolyte due to high anodization voltage (40 V) causing the burning of samples.

Figure 3b shows the SEM micrographs of TH-POM after second-stage hard anodization (HA) which was performed at constant voltage of 40 V in oxalic acid on pre-anodized samples at temperature $\leq 15^\circ\text{C}$. Well-ordered pores are obtained in HA samples as clearly visible in SEM image in Fig. 3b, and the desired ordered cylindrical pores having diameter ranging from 40 to 50 nm are shown in Fig. 3b (iii). SEM surface results of well-ordered pores are also confirmed by cross section/internal structure of the pores

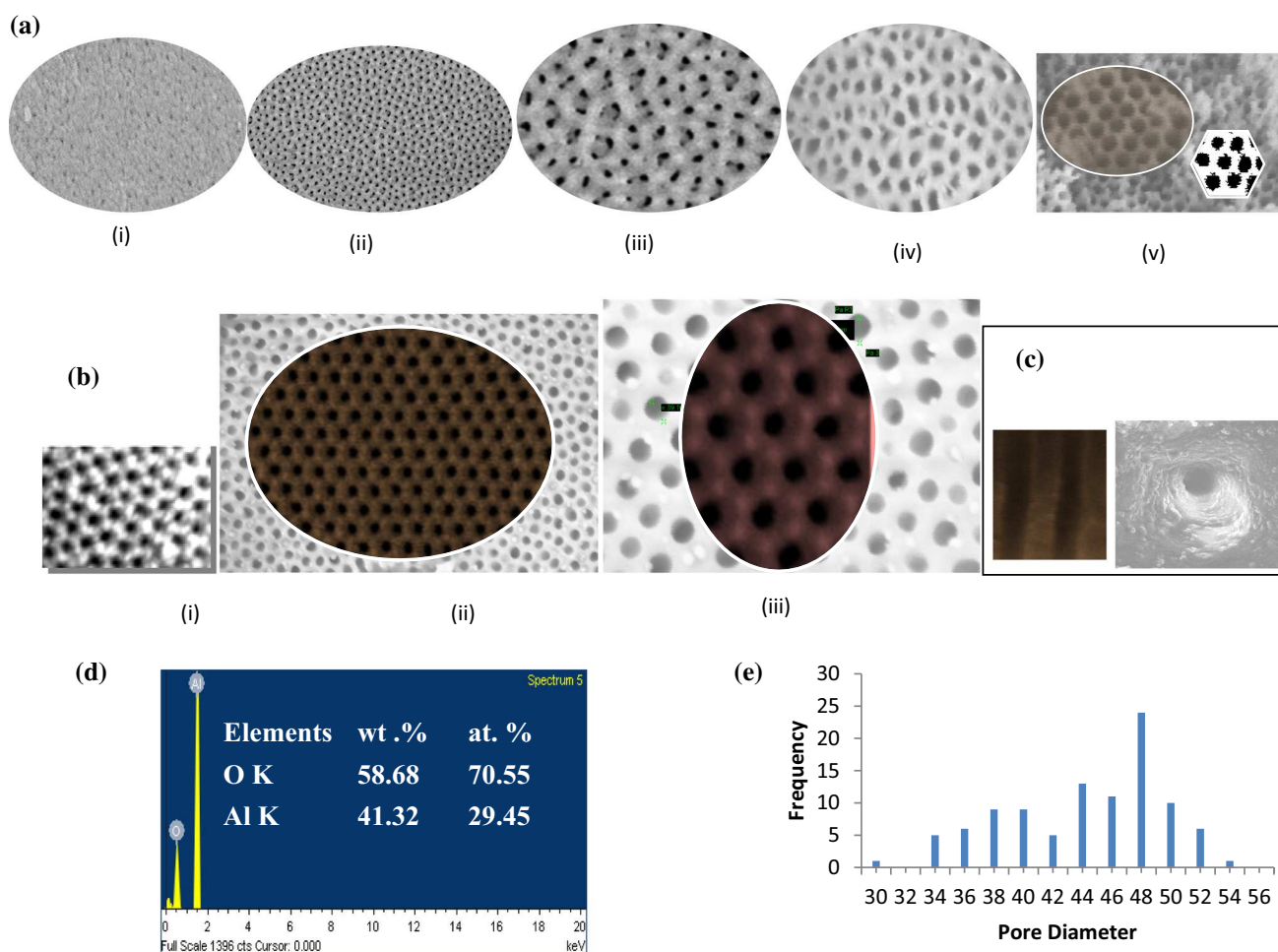


Fig. 3 SEM micrographs of anodized aluminum in **a** sulfuric acid (MA) at different time durations (i–iv) and low- and high-magnification images in (v); **b** HA in oxalic acid at different time durations

(i–iii), pore widening in (iii) also showing low- and high-magnification images (ii and iii); **c** cross-sectional/internal structure of pores; **d** EDS spectrum of Al_2O_3 ; **e** pore size distribution

in Fig. 3c. EDS analysis confirms the formation of Al_2O_3 as shown in Fig. 3d. Figure 3e shows the pore size distribution chart which was also obtained by considering 100 pores which shows that the maximum number of pores has size in the range from 45 to 48 nm. This range of pores is mainly required for the fabrication of metallic, composite, semiconductor nanowires, as they provide high surface-to-volume ratio and have a number of biological and chemical species detection and sensors applications [36]. Zhao et al. prepared alumina films by pulsed DC in a mixture of acids

at 15 °C but pores obtained are not ordered [37]. The pore diameter, interpore distance, porosity and pore density are calculated directly from SEM micrographs, and variation in relation to the time of anodization and type of electrolyte is presented in Table 2. Calculated result from SEM (presented in Table 2) estimated that the interpore distance of well-ordered pores after combined MA and HA is ~66 nm. Pore diameter increases from ~24 nm to 50 nm with enhancement in the porosity from 10 to 33% with change in electrolyte type, i.e., from MA to HA. Sanz et al. proved that values

Table 2 Results of anodized samples

Sample no.	Type of electrolyte	Time duration (min)	Pore diameter (nm)	Interpore distance (nm)	Porosity $\frac{\pi}{2\sqrt{3}} \left(\frac{D_{\text{pore}}}{D_{\text{interpore}}} \right)^2$	Pore density (cm^{-2})
1	Sulfuric	10	6–7	80	0.005 or 0.5%	$\sim 10^{14}$
2	Sulfuric	40	24–29	72	0.100 or 10%	7×10^{10}
3	Oxalic	120	40–50	66	0.332 or 33.2%	3×10^{10}

of all these parameters obtained by BET method [38] and BJH [39] method after N_2 adsorption were obtained from SEM images [40]. Interpore distance and pore diameter of anodized samples were calculated from FE-SEM top view images for different anodization timings.

Mechanism of pore formation is derived through the SEM results obtained for different samples in this study, and the results are discussed with the help of schematic diagram. Figure 4 shows the schematic diagram of the process of formation of pores deduced from the SEM images in Fig. 3a, b, and the related SEM results are also presented in Fig. 4. It is expected that the self-ordered pores form due to the repulsive forces between neighboring pores during anodization. There is formation of hexagonal-shaped cell with pore residing at center due to the first-step anodization in H_2SO_4 (Figs. 3a (v), 4a), and then, there is start of dissolution of Al_2O_3 surrounding the pore in this hexagonal cell (Fig. 4b, c). Then, there is start of formation of new pores under the effect of oxalic acid (HA) (Figs. 3b(i), 4d). After the formation of new pores, the pores are reshaped in a well-defined hexagonal pattern (Figs. 3b (ii), 4e). With the careful selection of electrolyte parameters and time duration of tests, pores are widened for required applications, and for this study, as discussed before required sized well-ordered nanopores are obtained with one pore surrounded by six

pores, which is shown schematically in Fig. 4f obtained with the help of actual pattern of pores obtained in Fig. 3b (iii). There complete mechanism of pore formation from the first-step mild anodization to the second-step hard anodization is shown in Fig. 4 which also shows the effect of change in electrolyte and anodization time duration. The potentiostatic current and applied potential reflect the formation of porous oxide membrane. Figure 5 shows measured current–time ($I-t$) and voltage–time ($V-t$) curves recorded during a 40 V anodization process. According to the AAO growth mechanism discussed by Lee et al., anodization process consists of two types of currents, i.e., ionic current and electronic current [41]. The ionic current is the main source of current flow, while electronic current can be overlooked since AAO template is an insulator. When the barrier oxide layer is thin, electric field is strong, thus diffusion of O^{2-} through oxide/Al interface is very fast, and this leads to oxidation of Al very fast and hence an increase in the barrier layer thickness and corresponding decrease in electric field. Diggle et al. reported that the ionic current density is related to electric field strength (E) with an exponential function [42];

$$J_{ion} = Xne^{YE} \quad (5)$$

where both X and Y are constants related to electrolyte temperature and n is the surface density of mobile ions.

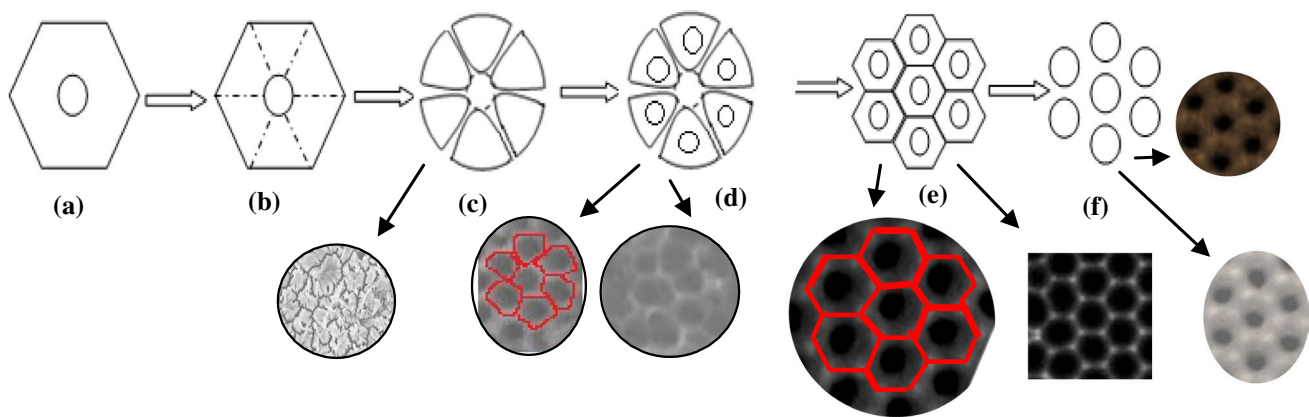
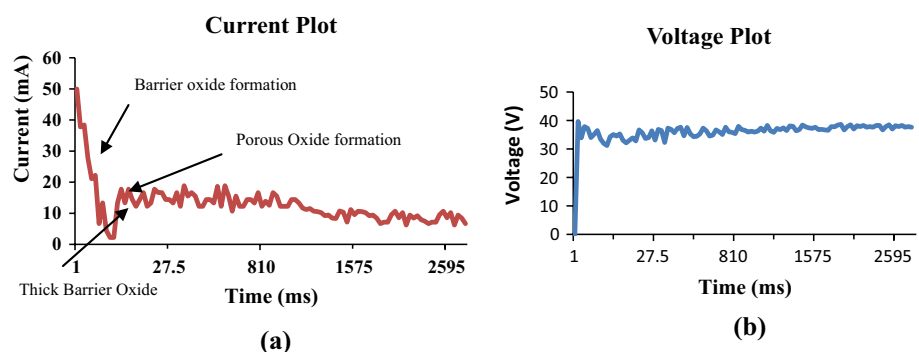


Fig. 4 Mechanism of pores formation with the help of schematic diagram along with actual SEM images

Fig. 5 **a** Current versus time curve; **b** voltage versus time curve during anodization process



Further anodizing the sample results in the formation of porous oxide that can be interpreted from Fig. 5a, current increases once again from minimum value. Finally a steady state pore structure is formed indicated by current saturation at longer duration of anodization. This can be attributed as the gradually reduction in concentration of hydrogen ions in electrolyte as a result of which dissolution rate and oxidation rate achieve balance. The anodization process is a balance procedure, and there exist two opposite processes: the forming of the anodic aluminum films and the dissolving of the films, Eqs. (8), (9) [32].

1. Al^{3+} ions formation at the metal/oxide interface,



2. The electrolysis of water increasing H^+ and O^{2-} , at electrolyte/oxide interface,



3. O^{2-} migration from electrolyte/oxide interface to oxide/metal interface and reaction with Al^{3+} due to electric field,



4. Dissolution of oxide at electrolyte/oxide interface,

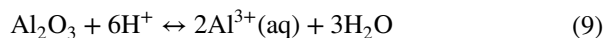


Figure 5b shows that applied voltage first increases because of the formation of nonporous oxide (barrier oxide) on the surface. As the thickness of oxide increases, there is also an increase in the resistance which increases the voltage to a maximum value of 39.6366 V. As the time of anodization increases, there may be some changes in the physical properties of oxide film which leads to the formation of pores by oxide dissolution. Due to dissolution of oxide, there is a decrease in the resistance of oxide layer, which decreases the voltage to 32 V as shown in Fig. 5b. Granulating curve between 34 and 36 V approximately suggests the formation and dissolution of the oxide process occurring at the bottom of the pores.

Before dissolving the remaining Al substrate opposite to the oxide layer, some samples were also undergone thermal stress treatment. It has been found that due to lower thermal expansion coefficient of Al_2O_3 , the oxide layer surface started cracking as shown in Fig. 6b at temperature above 95 °C. However, it was not able to peel off the oxide layer. Though the thermal stress treatment is done up to temperature of 150 °C, appearance of cracks from 95 °C indicates temperature performance range. The temperature-dependent behavior of the anodized membrane will be affected by various environment conditions, which is not in the scope of this study and may be tested by the researchers as per their required applications. This TH-POM will be used as

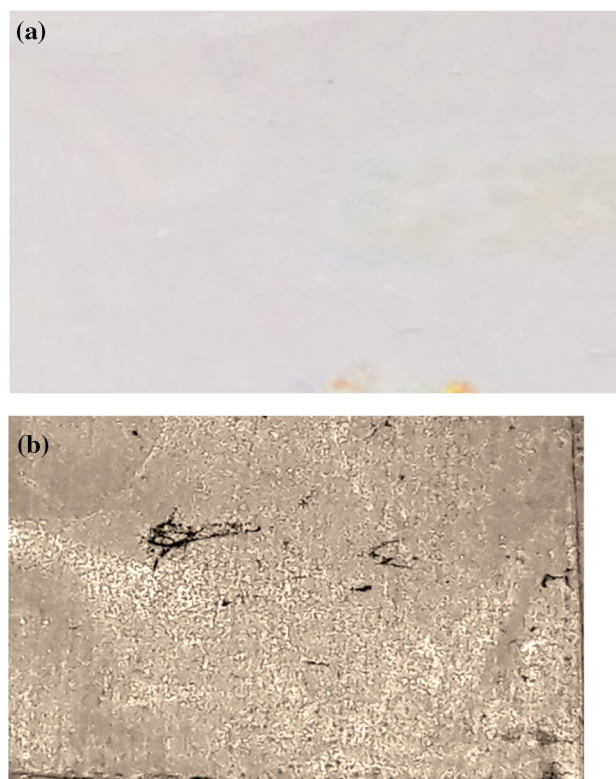


Fig. 6 Macrograph of **a** TH-POM obtained after removal of Al substrate; **b** top view of oxide layer after thermal stress treatment

a template for the growth of ordered nanowires for further application in enhancing the efficiency of flexible and transparent solar cells, and the various mechanical strength tests will be performed using equipments such as pin-on-disk as was done in previous works [43].

4 Conclusion

In this study, a novel combination of mild anodization–hard anodization with heterogeneous control parameters is used successfully to produce a well-ordered through-hole porous membrane for further various applications.

- It is observed from the pore size distribution chart that a maximum number of pores have size range from 45 to 48 nm.
- This experimental study is successful in the formation of well-ordered pores having 66-nm interpore distances with the high porosity of 33% in less time and without requiring costly equipments. The pore diameter is increased from 24 to 50 nm, while the porosity increased from 10 to 33% with a change in type of electrolyte.
- In coloring and finishing industries, for long hours of anodization at higher temperature the concentration

strength also changes due to the addition of Al cations and reduction of protons can affect the morphology of the formation of pores.

- The experimental procedure adopted in this study can be used for the anodization of other metals also and by varying the parameters such as addition of phosphoric acid which may further decrease the anodization time duration.

Acknowledgements The authors thankfully acknowledge the research grant sanctioned by the Science and Engineering Research Board, Department of Science and Technology, New Delhi, Government of India, under 'Fast Track Young Scientist-Engineering Science Scheme' vide No. SB/FTP/ETA-0366/2012, dated: 17.08.2015.

References

- Runge JM (2018) A brief history of anodizing aluminum. In: The metallurgy of anodizing aluminum, 1st edn. Springer International Publishing, Cham, pp 65–148
- Litong G, Junlong T, Jing W, Baoye L, Cheng X, Yabo Z, Yinghui Q (2013) Effect of anodization on titanium–porcelain bonding. *Mater Manuf Processes* 28(12):1305–1309
- Wu L, Liu J, Wu G, Li S, Yu M (2015) Growth behaviour of anodic oxide film on titanium alloy. *Surf Eng* 31(12):904–911
- Shetty A, Nanda K (2012) Synthesis of zinc oxide porous structures by anodization with water as an electrolyte. *Appl Phys A* 109(1):151–157
- Salman S, Okido M (2013) Anodization of magnesium (Mg) alloys to improve corrosion resistance. In: Song G-L (ed) *Corrosion prevention of magnesium alloys*. Woodhead Publishing, pp 197–231
- Mardare A, Ludwig A, Savan A, Hassel AW (2014) Properties of anodic oxides grown on a hafnium–tantalum–titanium thin film library. *Sci Technol Adv Mater* 15(1):1–11. <https://doi.org/10.1088/1468-6996/15/1/015006>
- Park S, Lee B (2004) Anodizing properties of high dielectric oxide films coated on aluminum by sol–gel method. *J Electroceram* 13(1–3):111–116
- Rezagholi H, Madar K, Mirjani M, Ahangarkani M (2014) Study on electropolished/anodised aluminium foil before and after dyeing. *Surf Eng* 30(3):165–171
- Hou P, Liu C, Shi C (2012) Carbon nanotubes prepared by anodic aluminum oxide template method. *Chin Sci Bull* 57(2–3):187–204
- Soltani N, Sadrnezhaad S, Bahrami A (2014) Manufacturing wear-resistant 10 Ce-TZP/Al₂O₃ nanoparticle aluminum composite by powder metallurgy processing. *Mater Manuf Processes* 29(10):1237–1244
- Nazari A, Saedodin S (2017) Porous anodic alumina coating for optimisation of pool-boiling performance. *Surf Eng* 33(10):753–759
- Radzik C, Kocanda G, Sheik M, Ballantine D (2008) Electrical impedance response of a thick–thin film hybrid anodic nanoporous alumina sensor to methanol vapors. *Int J Smart Sens Intell Syst* 1(2):470–479
- Ma Y, Kaczynski J, Ranacher C, Roshanghias A, Zauner M, Abasahl B (2018) Nano-porous aluminum oxide membrane as filtration interface for optical gas sensor packaging. *Microelectron Eng* 198:29–34
- Lu C, Huang Y, Huang J, Chang C, Wu S (2010) A macroporous TiO₂ oxygen sensor fabricated using anodic aluminum oxide as an etching mask. *Sensors* 10(1):670–683
- Song M, Zhou X, He X, Cao H, Liu J, Qiu H, Jin Z (2018) Distance dependent fluorescence enhancement of silver nanowires deposited on AAO. *Opt Mater* 83:241–244
- Cheng W, Zhou Y, Guan X, Hui Y, Wang S, Miao X (2016) Preparation and magnetic properties of FePt nanodot arrays sputtering on AAO templates. *Mater Manuf Processes* 31(2):173–176
- Sasagawa T, Kogut L (2011) Microelectromechanical devices and method utilizing a porous surface. US Patent 7944603, B2
- Sacco L, Florea I, Châtelet M, Cojocar C (2018) Investigation of porous anodic alumina templates formed by anodization of single-crystal aluminum substrates. *Thin Solid Films* 660:213–220
- Fan L, Guo D, Ren F, Fu Q, Jiang CZ (2008) Substrate grain boundary effects on the ordering of nanopores in anodic aluminum oxide. *Solid State Commun* 148(7–8):286–288
- Stepniowski WJ, Durejko T, Domanska MM, Lazinska M, Aniszewska J (2016) Characterization of nanoporous anodic aluminum oxide formed on laser pre-treated aluminum. *Mater Charact* 122:130–136
- Mauda H, Fukuda K (1995) Ordered metal nanohole arrays made by a two step replication of honeycomb structure of anodic alumina. *Science* 268:1466–1468
- Lv H, Liu S (2016) Preparation and analysis of porous anodic alumina template on silicon substrate. *Mater Manuf Processes* 31(2):157–161
- Maghsodi A, Adlnasab L, Shabanian M, Javanbakht M (2018) Optimization of effective parameters in the synthesis of nanopore anodic aluminum oxide membrane and arsenic removal by prepared magnetic iron oxide nanoparticles in anodic aluminum oxide membrane via ultrasonic-hydrothermal method. *Ultrason Sonochem*. <https://doi.org/10.1016/j.ultsonch.2018.07.003>
- Masuda H, Yamada H, Satoh M, Asoh H, Nakao M (1997) Highly ordered nanochannel-array architecture in anodic alumina. *Appl Phys Lett* 71(19):2770–2772
- Santos A, Montero-Moreno JM, Bachmann J, Nielsch K, Formentin P, Ferre-Borrull J, Pallares J, Marsal LF (2011) Understanding pore rearrangement during mild to hard transition in bilayered porous anodic alumina membranes. *ACS Appl Mater Interfaces* 3(6):1925–1932
- Lee W, Schwirn K, Steinhart M, Pippel E, Scholz R, Gosele U (2008) Structural engineering of nanoporous anodic aluminum oxide by pulse anodization of aluminum. *Nat Nanotechnol* 3:234–239
- Chu SZ, Wada K, Inoue S, Isogai M, Yasumori A (2005) Fabrication of ideally ordered nanoporous alumina films and integrated alumina nanotubule arrays by high-field anodization. *Adv Mater* 17:2115–2119
- Lee W, Ji R, Gosele U, Nielsch K (2006) Fast fabrication of long-range ordered porous alumina membranes by hard anodization. *Nat Mater* 5:741–747
- Liu J, Liu S, Zhou H, Xie C, Huang Z, Fu C, Kuang Y (2014) Preparation of self-ordered nanoporous anodic aluminum oxide membranes by combination of hard anodization and mild anodization. *Thin Solid Films* 552:75–81
- Xu TT, Piner RD, Ruoff R (2003) An improved method to strip aluminum from porous anodic alumina films. *Langmuir* 19(4):1443–1445
- Masuda H, Satoh M (1996) Fabrication of gold nanodot array using anodic porous alumina as an evaporation mask. *Jpn J Appl Phys* 35(Part 2 No.1B):126–129
- Electrochemistry of anodic alumina: Detailed equations. <https://sundoc.bibliothek.uni-halle.de/diss-online/04/04H055/t2.pdf>. Accessed 6 Jul 2018

33. Kushwaha MK (2014) A comparative study of different electrolytes for obtaining thick and well ordered nano-porous anodic aluminum oxide (AAO) films. *Procedia Mater Sci* 5:1266–1273
34. Surawathanawises K, Cheng X (2014) Nanoporous anodic aluminum oxide with a long-range order and tunable cell sizes by phosphoric acid anodization on pre-patterned substrates. *Electrochim Acta* 117:498–503
35. Chu SZ, Wada K, Inoue S, Todoroki S (2003) Fabrication of oxide nanostructures on glass by aluminum anodization and solgel process. *Surf Coat Technol* 169–170:190–194
36. Rajendra A, Parmar BJ, Sharma AK, Bhojraj H, Nayak MM, Rajanna K (2005) Hard anodisation of aluminium and its application to sensorics. *Surf Eng* 21(3):193–197
37. Zhao XX, Wei GY, Meng XF, Zhang A (2014) High performance alumina films prepared by direct current plus pulse anodization. *Surf Eng* 30(7):455–459
38. Brunauer S, Emmett PH, Teller E (1938) Adsorption of gases in multimolecular layers. *J Am Chem Soc* 60(2):309–319
39. Barrett EP, Joyner LG, Halenda PP (1951) The determination of pore volume and area distributions in porous substances. I. Computations from nitrogen isotherms. *J Am Chem Soc* 73(1):373–380
40. Sanz O, Echave FJ, Odriozola JA, Montes M (2011) Aluminum anodization in oxalic acid: controlling the texture of $\text{Al}_2\text{O}_3/\text{Al}$ monoliths for catalytic applications. *Ind Eng Chem Res* 50(4):2117–2125
41. Lee I, Jo Y, Kim Y, Tak Y, Choi J (2012) Electrochemical thinning for anodic aluminum oxide and anodic titanium oxide. *Bull Kor Chem Soc* 33(5):1465. <https://doi.org/10.5012/bkcs.2012.33.5.1465>
42. Diggle JW, Downie TC, Goulding C (1969) Anodic oxide films on aluminum. *Chem Rev* 69(3):365–405
43. Singh H, Khosla H, Walia GS, Sidhu TS, Kalsi SBS, Karthikeyan J (2018) Characteristic study of cold sprayed N06601 superalloy surface. *Surf Eng* 34(5):369–379

Publisher's Note Springer Nature remains neutral with regard to jurisdictional claims in published maps and institutional affiliations.